Surface stability of a bubble in a liquid fully confined in an elastic solid

Liu, YQ; Wang, Qian; zhang, aman

DOI:
10.1063/1.5055744

Document Version
Peer reviewed version

Citation for published version (Harvard):
Liu, YQ, Wang, Q & zhang, A 2018, 'Surface stability of a bubble in a liquid fully confined in an elastic solid', *Physics of Fluids*, vol. 30, no. 12, 127106. https://doi.org/10.1063/1.5055744

Surface stability of a bubble in a liquid fully confined by an elastic solid

Yunqiao Liu (刘筠乔)[1], Qianxi Wang (汪前喜)[2], A-Man Zhang (张阿漫)[3]

[1]Key Laboratory of Hydrodynamics (Ministry of Education), School of Naval Architecture, Ocean and Civil Engineering, Shanghai Jiao Tong University, Shanghai 200240, China

[2]School of Mathematics, University of Birmingham, Birmingham B15 2TT, UK

[3]College of Shipbuilding Engineering, Harbin Engineering University, Harbin, China

This paper is concerned with the surface stability of a bubble in a liquid, fully covered by an elastic solid, which is common in natural and engineering applications. A theoretical model is described for the phenomenon, assuming that the bubble gas undergoes a polytropic process, the flow is irrotational and the variation of the liquid volume is proportionally related to the liquid pressure. The boundary valued problem is modelled using the perturbation method via the Legendre polynomials and the evolution equations for radial and shape oscillations of a confined bubble are formulated. We derive an explicit analytical expression for the natural frequency of shape modes for a confined bubble. The analyses lead to interesting conclusions including: The natural frequency of shape mode increases due to the confinement only if the cavity dimension is within 2-3 bubble radii, for which the shape oscillation of a bubble is always stable and damps with time; as the cavity dimension is 10 times larger than the bubble radius, the natural frequency for radial oscillation is significantly larger while the natural frequency for shape mode remains the same as that for an unconfined bubble; the influence of confinement on the natural frequency decreases with mode number. An unconfined bubble experiences shape mode oscillation under the Mathieu relation. In contrast, shape mode resonance of confined bubbles occurs only when both the radial resonance condition and the Mathieu relation are satisfied, which is associated with a much larger driving frequency of ultrasound.

Key words: Bubble dynamics in confined liquid; Shape oscillation; Natural frequency

Nomenclature

a_k Amplitude of k-th shape mode

k Mode number of shape mode

K Bulk modulus

p Pressure

p_B pressure inside bubble

p_g pressure of gas

p_{sat} pressure of saturated vapor

$P_k(\cos\theta)$ Legendre polynomials

r_b Radial component of bubble surface

R_b Mean radius of bubble

R_c Radius of cavity

S Surface shape function of bubble

V Volume

α Natural frequency ratio of confined bubble to unbounded bubble

β Ratio of cavity radius to bubble radius

φ Velocity potential

ε Dimensionless amplitude of acoustic wave

ρ Density

μ Viscosity

Γ Polytrophic index

γ Surface tension

ω Frequency

ω_d Driving frequency

Subscript

0 Initial state

b Bubble

c Cavity or confinement wall

eq Equilibrium state

l Liquid

1. Introduction

Surface mode oscillations or shape oscillations, are associated with the stability of a bubble and present an importance issue in bubble dynamics. Unstable shape oscillations bring about inertial collapse, causing noise and erosion to fluid machinery (Knapp et al. 1970). As contrast enhancing agents in ultrasound imaging, stable shape oscillations of bubbles contribute to the acoustic signal, which is different from the one yielded by blood vessel, so as to enhance blood-tissue contrast to improve the quality of image of blood vessels in sonography (Dollet et al. 2008). In this case, the contrast-agent bubbles are expected to exist as long as possible in order to elongate imaging time. The stability of the bubbles determines their residence time. Having a better understanding of surface mode oscillations of bubbles leads to a greater knowledge of the stable/unstable conditions.

The bubbles are confined in vessels in the above medical applications. Actually, confined bubbles are more widely found and utilized. For example, the expulsion of the spores of some special types of ferns is related to the dynamics of confined bubbles (Noblin et al. 2012). The bubbles in the liquids entrapped in rocks can provide information on the history of thermodynamic conditions (Roedder 1980; Marti et al. 2012). Also, during droughts, cavitation bubbles may form and be confined in plant vessels that convey water to various parts of the plant and damage the plant xylem, which is deemed as a reason for the death of plants (Tyree & Sperry 1989; Cochard 2006). Studies in plant science associated with cavitation and acoustic wave emission in plant xylem, especially that on drought-induced plant stress, are getting growing attention over recent years (de Roo et al. 2016). In addition, bubbles are increasingly being utilized in microfluidic systems where their confined dynamics are of crucial importance to device operation (Marmottant & Hilgenfeldt 2004, Soltani et al. 2018). Therefore, a complete understanding of the surface mode oscillations of a bubble should include the effects of confinement.

Interesting similarity exists between surface mode of bubbles and a free surface wave on a water surface (Lamb 1932; Lauterborn & Kurz 2010). This viewpoint starts from a flat horizontal surface dividing liquid and gas into two half spaces, with the gas filling the upper half space. Wrapping the liquid upwards to enclose a blob of gas leads to a bubble surrounded by the liquid. A small amplitude wave on the flat surface will become a small amplitude surface mode on the bubble. The periodic boundary conditions thereby impose definite frequencies for standing waves (shape oscillations) (Lauterbon & Kurz 2010). Free surface waves in a finite water depth are analogous to shape modes of a bubble in a confined cavity, and are significantly affected by the water depth. We are wandering if the shape mode oscillation of a bubble is affected by a confined cavity.

Existing studies on shape oscillations are mostly for a bubble suspended in an infinite unbounded liquid without confinement (Plesset & Prosperetti 1977, Feng & Leal 1997; Brenner et al. 2002; Lauterborn & Kurz 2010). For unbounded bubbles, the Rayleigh-Taylor instability and the Mathieu instability are two typical mechanisms to induce shape instability (Hilgenfeldt et al. 1996). The former is the instability of an interface between two fluids of different densities which occurs when the lighter fluid is pushing the heavier fluid, occurring after the bubble radius reaches its minimum and the gas accelerates rapidly into the liquid (Sharp 1984). The typical time scale of the Rayleigh-Taylor instability is of the order of nanoseconds. The latter is related to the parametric instability (Benjamin 1964), yielding when the driving frequency of the acoustic wave, ω_d, and the natural frequency of shape modes, ω_k, satisfies the Mathieu relation $2\omega_k/\omega_d = n$, where n is a natural number. The most unstable situations are for $n = 1$ or 2, namely one-two and one-one resonances, respectively (Feng & Leal 1993; Yang, Feng & Leal 1993). The time scale of the Mathieu instability is of the order of microseconds, much longer than that of the Rayleigh-Taylor instability. Experimental investigations of shape oscillations of bubbles are reported by Asaki et al. (1993, 1995). The detailed process of shape oscillation of micron-sized single air bubbles is captured by Versluis et al. (2010) using high speed camera. In this work, we endeavour to figure out the mechanism of shape instability for confined bubbles.

We are concerned with the oscillation of the bubble shape within a liquid-filled cavity completely covered by an elastic solid. To reduce the complexity in the mathematical analysis, assumptions are made that the cavity and the bubble are spherical and concentric at the beginning. The features of the confined bubbles or cavities in non-concentric situations can be qualitatively indicated by that of this special case (Martynov et al. 2009). Numerical models for more general cases can be validated using the outcome of this work.

In this paper, a simple model is established to deal with the variations of pressure and volume in bubble gas, the ambient liquid motion, the cavity deformation and the interactions of the above. The gas in bubble is assumed to comply with adiabatic or isothermal conditions. In a confined space, the liquid pressure variation caused by bubble oscillation reaches a much greater extent. In the non-dimensionalized equation of continuity, the effect of water compressibility was demonstrated to be insignificant (Wang 2017). Therefore, we use incompressible continuity equation for the liquid motion, and the relationship between the pressure on the cavity surface and the liquid volume or the cavity volume is proportional. The governing equations are expanded in terms of the Legendre polynomials and the evolution equations for shape oscillations of the confined bubble are formulated.

In Sec. 2, we derive an explicit expression for the natural frequency of shape modes for a confined bubble. In Sec. 3, we analyse the effects of confinement on the frequency of shape modes along with the stability of shape modes in confinement. Two types of surface instabilities, the Rayleigh-Taylor instability and the parametric instability, are observed for confined bubbles. Concluding remarks are given in Sec. 4.

2. Physical and mathematical modelling

2.1 Dynamic equations

Figure 1 shows the schematic graph of a bubble confined in an elastic cavity filled with liquid. The system is composed of the elastic solid covering the cavity, the liquid between the cavity and the bubble, and the gas/vapor in the bubble. For the convenience of mathematical analysis, the cavity and the bubble are taken as spherical and concentric at the beginning. $R_c(t)$ represents the instantaneous cavity radius, and the instantaneous radial coordinate of the bubble interface as $r_b(\theta, t)$, where θ is the angular coordinate.

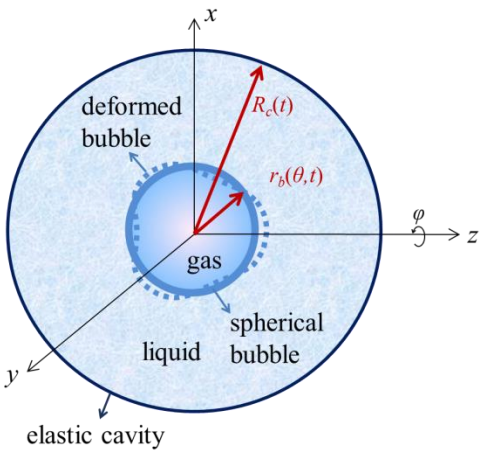

Figure 1. Schematic graph of the system where a gas bubble is confined in a cavity with elastic solid boundary that is concentric with the bubble. The cavity radius is denoted as $R_c(t)$ and the bubble surface $r_b(\theta, t)$.

We assume that the bubble is approximately spherical, while undergoing nonlinear radial oscillation and shape oscillations with small amplitude. The shape perturbation to a spherical bubble can be expanded in terms of the spherical harmonics. With the restriction to axisymmetric deformation, which is applied in the present work for simplicity, the spherical harmonics reduce to the Legendre polynomials $P_k(\cos\theta)$. Thus, the bubble surface can be expressed as **(Plesset 1954)**

$$r_b(\theta,t) = R_b(t) + \sum_{k=2}^{\infty} a_k(t) P_k(\cos\theta)\,, \tag{2.1}$$

where ***R_b* is the mean radius,** and a_k is the amplitude of the k-th order surface mode, assuming $a_k(t) << R_b(t)$. It is noted that the summation is from $k = 2$ since $k = 1$ is related to the translation of the non-deformed bubble and is not considered here. The volume of the bubble V_b is calculated to be

$$V_b = \frac{2\pi}{3}\int_0^{\pi} {r_b}^3 \sin\theta d\theta = \frac{4\pi}{3}R_b^3 + \frac{12}{15}R_b a_2^2 + \frac{12}{21}R_b a_3^2 + \frac{4}{9}R_b a_4^2 + O(R_b a_k^2) + O(a_k^3)\,, \tag{2.2}$$

which implies the change of volume due to shape modes is at the order of $O(R_b a_k^2)$ and higher, and thus neglected hereafter. Another assumption is that the cavity volume, V_c, is much larger than that of the bubble, i.e. $V_c/V_b >> 1$. Thus, the relationship between the variation of the pressure at confinement wall and the cavity volume is regarded as linear **(Vincent & Marmottant 2017).**

$$p_c - p_0 = K_c \frac{V_c - V_{c0}}{V_{c0}}\,, \tag{2.3}$$

where p_c and p_0 are the transient liquid pressure at confinement wall and the initial liquid pressure, respectively, ***V_{c0}* is the initial cavity volume,** and K_c is the bulk modulus of the elastic confinement. **Since the volume change due to the shape modes is neglected as mentioned above, merely the shape mode does not change the stiffness of the system according to Eq. (2.3). Therefore, the cavity could keep spherical and the pressure on the cavity p_c does not depend on θ.**

The compressibility effects of water in the continuity equation can be neglected, i.e. $\nabla\cdot\mathbf{u} = 0$ (Wang 2017). Using the dimensionless analysis, it has been shown that the compressibility effects in the continuity equation are of the order of 0.01, when the variation amplitude of the liquid pressure is at 20 MPa. However, a small change in liquid volume may lead to the significant pressure variation. The liquid volume is deemed to vary proportionally to the pressure on the confinement boundary **(Vincent & Marmottant 2017)**

$$p_c - p_0 = K_l \frac{V_{l0} - V_l}{V_{l0}}\,, \tag{2.4}$$

where K_l is the bulk modulus of water, and V_{l0} and V_l are the initial and the transient volumes of the liquid, respectively.

The total volume of the bubble and the liquid combined equals to that of the cavity **(Wang 2017),**

$$V_b + V_l = V_c\,, \qquad V_{b0} + V_{l0} = V_{c0}\,, \tag{2.5}$$

where the transient and the initial volume of the bubble are denoted as V_b and V_{b0}, respectively. From equation (2.3-2.5) we have

$$V_b - V_{b0} = \frac{1}{K_c}(p_c - p_0)V_{c0} + \frac{1}{K_l}(p_c - p_0)V_{l0}\,. \tag{2.6}$$

The assumption of $V_{c0} >> V_{b0}$ leads to **(Vincent & Marmottant 2017)**

$$\frac{V_b - V_{b0}}{V_{c0}} = \left(\frac{1}{K_l} + \frac{1}{K_c}\right)(p_c - p_0)\,, \tag{2.7}$$

or

$$p_c - p_0 = \frac{K}{V_{c0}}(V_b - V_{b0})\,, \qquad K = \frac{K_l K_c}{K_l + K_c}\,, \tag{2.8}$$

where K is defined as the effective bulk modulus for the system. K grows with K_l, the liquid bulk modulus and K_c, the confinement bulk modulus. Equation (2.8) can be approximated according to Eq. (2.2) as,

$$p_c - p_0 = \frac{K}{R_{c0}^3}(R_b^3 - R_{b0}^3)\,. \tag{2.9}$$

The velocity potential satisfying Laplace's equation is expressed based on an axisymmetric spherical coordinate as,

$$\varphi(r,\theta,t) = \frac{A_0(t)}{r} + B_0(t) + \sum_{k=2}^{\infty}\left[\frac{A_k(t)}{r^{k+1}} + B_k(t)r^k\right]P_k(\cos\theta)\,, \tag{2.10}$$

where $A_k(t)$ and $B_k(t)$ are coefficients to be determined from the kinematic boundary conditions

$$\frac{\partial S}{\partial t} + (\nabla\varphi\cdot\nabla)S = 0\,, \tag{2.11}$$

where S is the surface shape function, defined at the bubble interface as

$$S \equiv S_b = r - R_b(t) - \sum_{k=2}^{\infty} a_k(t)P_k(\cos\theta)\,, \tag{2.12}$$

and at the confinement as

$$S \equiv S_c = r - R_c(t)\,. \tag{2.13}$$

By substituting **Eqs.** (2.10) and (2.12) or (2.13), the second term of **Eq.** (2.11) is written as

$$(\nabla\varphi\cdot\nabla)S = \frac{\partial\varphi}{\partial r}\frac{\partial S}{\partial r} + \frac{1}{r}\frac{\partial\varphi}{\partial\theta}\frac{1}{r}\frac{\partial S}{\partial\theta} = -\frac{A_0}{r^2} + \sum_{k=2}^{\infty}\left[-(k+1)\frac{A_k}{r^{k+2}} + kB_k r^{k-1}\right]P_k(\cos\theta)\,, \tag{2.14}$$

where the higher order terms, following the multiplication of the Legendre polynomials, are eliminated **(see Appendix A)**. Writing the kinematic boundary condition explicitly at the bubble interface and at the confinement, respectively, we obtain

$$-\frac{A_0}{R_b^{\,2}}+\sum_{k=2}^{\infty}\left[\frac{2A_0}{R_b^{\,3}}a_k-(k+1)\frac{A_k}{R_b^{\,k+2}}+kB_kR_b^{\,k-1}\right]P_k(\cos\theta)=\dot{R}_b+\sum_{k=2}^{\infty}\dot{a}_kP_k(\cos\theta), \tag{2.15}$$

$$-\frac{A_0}{R_c^{\,2}}+\sum_{k=2}^{\infty}\left[-(k+1)\frac{A_k}{R_c^{\,k+2}}+kB_kR_c^{\,k-1}\right]P_k(\cos\theta)=\dot{R}_c. \tag{2.16}$$

Combining the above two equations and making use of the orthogonality of the Legendre polynomials, we obtain

$$A_0=-\dot{R}_bR_b^{\,2}=-\dot{R}_cR_c^{\,2}, \tag{2.17}$$

$$-\frac{2\dot{R}_b}{R_b}a_k-(k+1)\frac{A_k}{R_b^{\,k+2}}+kB_kR_b^{\,k-1}=\dot{a}_k, \tag{2.18}$$

$$-(k+1)\frac{A_k}{R_c^{\,k+2}}+kB_kR_c^{\,k-1}=0. \tag{2.19}$$

Combining Eqs. (2.18) and (2.19) results in

$$A_k=\frac{R_b^{\,k+1}R_c^{\,2k+1}(\dot{a}_kR_b+2a_k\dot{R}_b)}{(k+1)(R_b^{\,2k+1}-R_c^{\,2k+1})}, \tag{2.20a}$$

$$B_k=\frac{R_b^{\,k+1}(\dot{a}_kR_b+2a_k\dot{R}_b)}{k(R_b^{\,2k+1}-R_c^{\,2k+1})},\ \text{for } k\geq 2. \tag{2.20b}$$

The coefficients A_k and B_k are thus at the same order of a_k. The coefficient B_0 is a constant and does not affect the results as the velocity is proportional to the potential gradient.

If we substitute A_k and B_k into the expression of velocity potential (2.10) and evaluate it at $r = R_c$, the velocity potential due to the shape mode becomes

$$\left.\frac{A_k}{r^{k+1}}+B_kr^k\right|_{r=R_c}=-\frac{2k+1}{k(k+1)}\frac{\beta^k}{\beta^{2k+1}-1}\left(R_b\dot{a}_k+2\dot{R}_ba_k\right) \tag{2.21}$$

where $\beta=R_c/R_b$ is the confinement ratio. If β is much larger than 1, which is true for the present work, Eq. (2.21) approaches to zero. Therefore, the dynamic pressure due to shape mode can be neglected at the cavity, and it is reasonable to assume the pressure on the cavity p_c is uniform spatially and independent on θ.

The Bernoulli equation for the liquid flow reads

$$\rho\left(\frac{\partial\varphi}{\partial t}+\frac{1}{2}|\nabla\varphi|^2\right)_{S_b}+p_{lb}=\rho\left(\frac{\partial\varphi}{\partial t}+\frac{1}{2}|\nabla\varphi|^2\right)_{S_c}+p_c, \tag{2.22}$$

where p_{lb} is the liquid pressure at the bubble interface, related to the pressure inside the bubble p_B based on the dynamic boundary condition (Plesset & Prosperetti 1977):

$$-p_{lb}-p_A+2\mu\frac{\partial^2\varphi}{\partial r^2}=-p_B+\gamma\nabla\cdot\mathbf{n}\,, \tag{2.23}$$

where p_A is the acoustic pressure applied at the position of the bubble, μ is the liquid viscosity and γ is the surface tension. Equation (2.23) describes the stress balance of the pressure difference, viscous stress and surface tension. The bubble pressure p_B includes partial pressure of saturated vapor p_{sat}, which is provided as a constant, and partial pressure of gas p_g which changes according to the polytrophic law (Plesset & Prosperetti 1977)

$$p_B = p_{sat} + p_{g0}\left(\frac{R_{b0}}{R_b}\right)^{3\Gamma}, \tag{2.24}$$

where p_{g0} is the gas pressure which will be given as an initial condition, Γ is the polytrophic index of the bubble gas. The last term in Eq. (2.23) is associated with the surface tension, written as

$$\gamma\nabla\cdot\mathbf{n}=\frac{2\gamma}{R}+\gamma\sum_{k=2}^{\infty}(k+2)(k-1)\frac{a_k}{R^2}P_k(\cos\theta)\,. \tag{2.25}$$

Substituting the expansion (2.10) for the velocity potential into Bernoulli's equation (2.22) and expanding in terms of the Legendre polynomials, we obtain the dynamic equation of radial motion of the bubble, which is associated with the zeroth-order Legendre polynomial ($k = 0$)

$$R_b\ddot{R}_b+\frac{3}{2}\dot{R}_b^{\,2}+\frac{p_c-p_g-p_A}{\rho}+\frac{2\gamma}{\rho R_b}+\frac{4\mu\dot{R}_b}{\rho R_b}-\frac{2R_b\dot{R}_b^{\,2}+R_b^{\,2}\ddot{R}_b}{R_c}+\frac{R_b^{\,4}\dot{R}_b^{\,2}}{2R_c^{\,4}}=0\,, \tag{2.26}$$

which is consistent with Fourest et al. (2014). The variation of the pressure at the confinement, p_c, is given by Eq. (2.9). The transient radius of the confinement is determined by

$$R_c^3-R_{c0}^3=\frac{K}{K_c}(R_b^3-R_{b0}^3)=\frac{K_l}{K_c+K_l}(R_b^3-R_{b0}^3)\,. \tag{2.27}$$

The dynamic equation of shape mode ($k \geqslant 2$) for the bubble is

$$
\begin{aligned}
&\ddot{a}_k \frac{(k+1)-(2k+1)\beta^k+k\beta^{2k+1}}{k(\beta^{2k+1}-1)} \\
&+\dot{a}_k \frac{2(k+1)\mu[(k-1)+(k+2)\beta^{2k+1}]}{\rho R_b{}^2(\beta^{2k+1}-1)} \\
&+\dot{a}_k \frac{\dot{R}_b}{kR_b(\beta^{2k+1}-1)^2}\begin{bmatrix} -3(k+1)+k(2k+1)\beta^{k-3}-(2k+1)(k-3)\beta^k \\ -(2k+1)^2\beta^{2k-2}+4(k^2+k+1)\beta^{2k+1} \\ +(2k+1)(k+1)\beta^{3k-2}-(2k+1)(k+4)\beta^{3k+1}+3k\beta^{4k+2} \end{bmatrix} \\
&+a_k \begin{bmatrix} \frac{\gamma(k-1)(k+1)(k+2)}{\rho R_b{}^3} \\ +\frac{4(k+1)\mu[(k+2)+(k-1)\beta^{2k+1}]\dot{R}_b}{\rho R_b{}^3(\beta^{2k+1}-1)} \\ +\frac{2(2k+1)(1-\beta^3)[k\beta^{k-3}-(2k+1)\beta^{2k-2}+(k+1)\beta^{3k-2}]R_b{}^3\dot{R}_b{}^2}{k(\beta^{2k+1}-1)^2} \\ +\frac{[(k+1)(k+2)-2(2k+1)\beta^k-(k-1)k\beta^{2k+1}]\ddot{R}_b}{kR_b(\beta^{2k+1}-1)} \end{bmatrix} = 0\,,
\end{aligned}
\tag{2.28}
$$

If the confinement ratio $\beta \to \infty$, Eq. (2.28) becomes

$$
\ddot{a}_k + \left[\frac{3\dot{R}_b}{R_b} + \frac{2(k+1)(k+2)\mu}{\rho R_b{}^2}\right]\dot{a}_k + (k-1)\left[-\frac{\ddot{R}_b}{R_b} + \frac{\gamma(k+1)(k+2)}{\rho R_b{}^3} + \frac{4(k+1)\mu\dot{R}_b}{\rho R_b{}^3}\right]a_k = 0\,, \tag{2.29}
$$

which is a well-known equation for the shape oscillation of a bubble in an unbounded fluid (Feng & Leal 1997). The detailed derivation of the dynamic conditions Eqs. (2.26) and (2.28) are referred to Appendix B.

2.2 Natural frequencies

Supposing the bubble oscillates around its equilibrium radius at an infinitesimal amplitude $R(t) = R_{beq}[1+x(t)], \quad (x(t) << 1)$ and linearizing **Eq.** (2.26), we obtain the natural frequency of the radial mode

$$
\omega_0 = \sqrt{\frac{1}{1-\beta_{eq}^{-1}}\left[\frac{3\Gamma p_{eq}}{\rho R_{beq}^2} + \frac{(6\Gamma-2)\gamma}{\rho R_{beq}^3} + \beta_{eq}^{-3}\frac{3K}{\rho R_{beq}^2}\right]}\,, \tag{2.30}
$$

where $\beta_{eq} = R_{ceq}/R_{beq},\ \beta_{eq} > 1,$ is the confinement ratio at equilibrium state. The equilibrium bubble radius is determined by

$$
p_{g0} = p_{eq} + p_{sat} + \frac{2\gamma}{R_{beq}}\,, \tag{2.31}
$$

where p_{eq} is the liquid pressure for the equilibrium state. As $\beta_{eq} = R_{ceq} / R_{beq} \to \infty$, we have $\omega_0 = \omega_{0\infty}$, where $\omega_{0\infty}$ is the natural frequency of radial mode for a bubble in an unbounded liquid (Minnaert 1933)

$$\omega_{0\infty} = \sqrt{\frac{3\Gamma p_{eq}}{\rho R_{beq}^2} + \frac{(6\Gamma - 2)\gamma}{\rho R_{beq}^3}} \ . \tag{2.32}$$

For a bubble of constant volume at equilibrium $R_b = R_{beq}$ ($\dot{R}_{beq} = 0$), we have $R_c = R_{ceq}$ ($\dot{R}_{ceq} = 0$), hence the confinement does not change shape. Using these conditions, the shape oscillation equation (2.28) becomes:

$$\frac{k\beta_{eq}^{2k+1} - (2k+1)\beta_{eq}^k + k + 1}{k(\beta_{eq}^{2k+1} - 1)} \ddot{a}_k + \frac{\gamma(k-1)(k+1)(k+2)}{\rho R_{beq}^3} a_k = 0, \tag{2.33}$$

from which we know the natural frequency of the shape mode is

$$\omega_k = \sqrt{\frac{k(\beta_{eq}^{2k+1} - 1)}{k\beta_{eq}^{2k+1} - (2k+1)\beta_{eq}^k + k + 1} \frac{\gamma(k-1)(k+1)(k+2)}{\rho R_{beq}^3}} \ . \tag{2.34}$$

As $\beta_{eq} = R_{ceq} / R_{beq} \to \infty$, we have $\omega_k = \omega_{k\infty}$, where $\omega_{k\infty}$ is the natural frequency of mode k for a bubble in an unbound liquid (Lamb 1932)

$$\omega_{k\infty} = \sqrt{\frac{\gamma(k-1)(k+1)(k+2)}{\rho R_{beq}^3}} \ . \tag{2.35}$$

3. Results and discussion

3.1 Effects of confinement on natural frequencies

We define the ratio of natural frequencies for confined bubble and unbounded bubble, α_k, as

$$\alpha_k = \omega_k / \omega_{k\infty} \ . \tag{3.1}$$

For the radial mode, α_k ($k = 0$) is calculated by **Eqs.** (2.30) and (2.32); for the shape modes α_k ($k \geqslant 2$) is given as following from **Eqs.** (2.34, 2.35)

$$\alpha_k = \sqrt{\frac{k(\beta_{eq}^{2k+1} - 1)}{k\beta_{eq}^{2k+1} - (2k+1)\beta_{eq}^k + k + 1}}, \quad (k \geq 2). \tag{3.2}$$

Referring to Eq. (2.28), we know that the natural frequency ratio α_k comes out from the coefficient of $\ddot{a}_k$, which is related to the added mass of the oscillatory system. The enlargement of the natural frequency of the shape mode can thus be regarded as the decrease of the added mass due to confinement.

Figure 2 displays the ratio of the natural frequency α_k in terms of the confinement ratio of the equilibrium radii, $\beta_{eq} = R_{ceq} / R_{beq}$, for a bubble with equilibrium radius R_{beq} = 5 μm, which is a typical size in medical ultrasound (Bjerknes et al. 1997). The parameters are chosen according to the standard water-gas system with liquid density ρ = 1000 kg·m^{-3}, viscosity $\mu = 1\times10^{-3}$ kg (m·s)$^{-1}$, surface tension γ = 0.0729 N·m^{-1}, and polytropic index Γ = 1.4. The equilibrium pressure is set as $p_{eq} = 10^5$ Pa. The bulk moduli of the confinement and liquid are given as K_c = 1 GPa, K_l = 2.2 GPa, respectively and the effective bulk modulus for the system as K = 0.7 GPa (Vincent et al. 2014).

As shown in Fig. 2(a), the natural frequency for the radial mode (k = 0) when $\beta_{eq} < 5$ is one order of magnitude larger than that without confinement, and decreases rapidly with β_{eq}. Similarly, the frequencies for shape modes ($k \geqslant 2$) increase due to the confinement and decrease with β_{eq} (Fig. 2(b)). The enlargement ratio of the natural frequency of shape mode is relatively small but still appreciable. In the present case, the detuning of the natural frequency is 10% due to confinement if the ratio β_{eq} is around 2.5. The change of the natural frequency due to the confinement is less than 1% when $\beta_{eq} \geq 88$ for spherical mode, k = 0, and $\beta_{eq} \geq 5$ for shape mode, k = 2, respectively.

As a bubble oscillates in water in a cavity, it causes compression and expansion of the water and the cavity boundary. The bulk modulus of water and the confinement are large. The stiffness of a confined bubble system thus increases significantly compared to an unconfined bubble. As a result, the frequency of the radial or volume oscillation of a confined bubble increases significantly. The frequency of the shape mode increases at a much smaller amplitude, since it is associated with the second order change of the bubble volume (see Eq. (2.2)).

In addition, the influence of confinement on the natural frequency decreases with mode number k, as shown in Figs. 2(b & c). According to Eq. (2.1), k is substantially the wave number along the bubble surface. As k increases, the wavelength decreases, so does its ratio to the characteristic length of confinement R_c. As a result, the effects of confinement on the shape mode decrease with k, being negligible for the shape mode $k \geq 10$ (Fig. 2c).

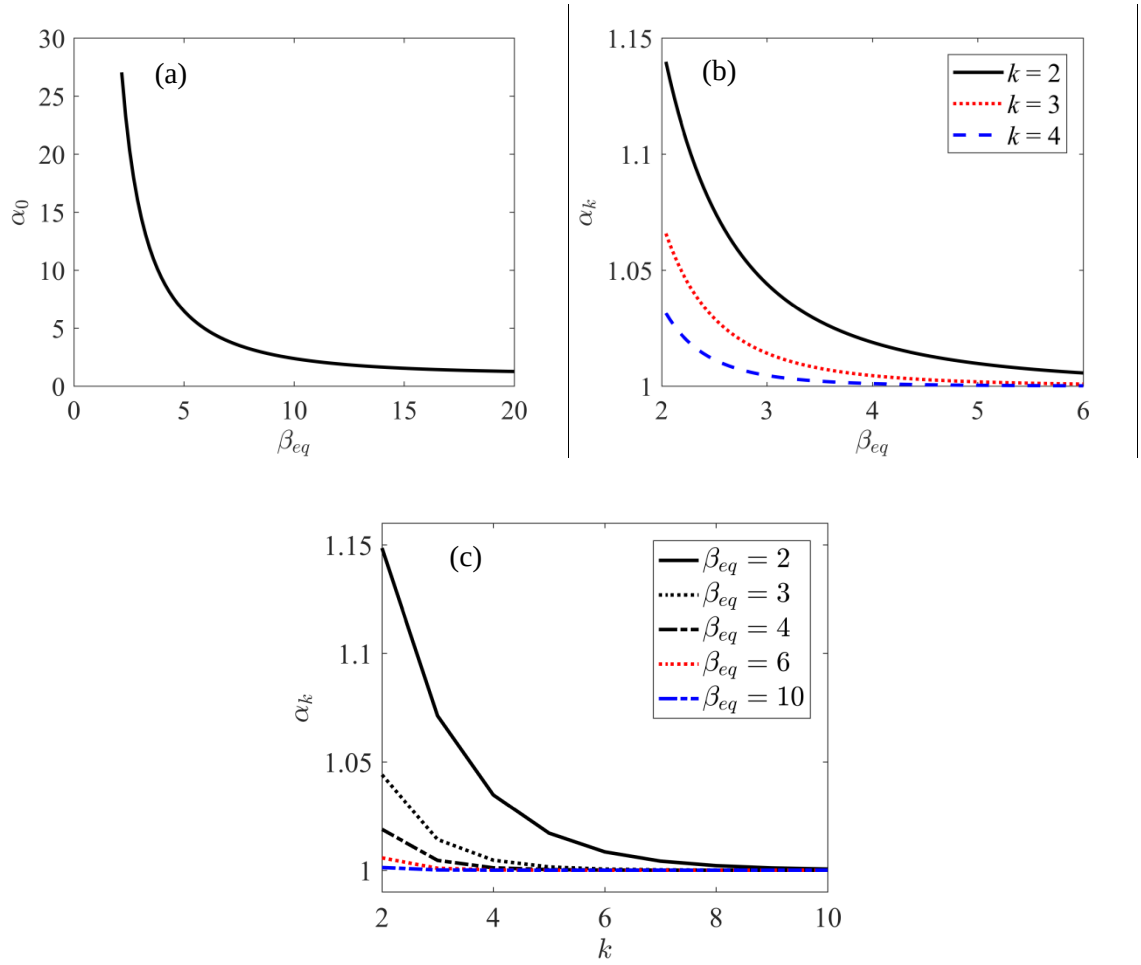

Fig. 2. Natural frequency ratio $\alpha_k = \omega_k / \omega_{k\infty}$ versus confinement ratio $\beta_{eq} = R_{ceq} / R_{beq}$: (a) radial mode and (b) shape modes. (c) Natural frequency ratio α_k versus shape mode order k for β_{eq} = 2, 3, 4, 6 and 10. R_{eq} = 5 μm, γ = 0.0729 N·m^{-1}, ρ = 1000 kg·m^{-3}, $\mu = 1\times10^{-3}$ kg (m·s)$^{-1}$, Γ = 1.4, $p_0 = 10^5$ Pa and K = 0.7 GPa.

3.2 Confined bubbles subject to an acoustic wave

To investigate the resonant mechanism of the surface instability, we consider the oscillation of a confined bubble at equilibrium initially subject to an acoustic wave, defined as following

$$p_A = p_{eq}[1+\varepsilon\sin(\omega_d t)] \ , \tag{3.3}$$

where ε is the dimensionless amplitude and ω_d is the driving frequency, which is set as ε = 1 in the present section to provide a consistent ultrasound intensity. Table 1 displays the natural frequencies of radial mode and shape modes (k = 2, 3 and 4) for the bubble with initial and equilibrium radius $R_0 = R_{eq}$ = 5 μm, which are calculated by Eqs. (2.30, 2.34) or (2.32, 2.35) for β_0 = 2.5, 10 and ∞. As shown in Table 1, the natural frequencies of shape modes increase appreciably due to confinement only for β_0 = 2.5, while the natural frequency of radial mode changes dramatically from β_0 = 2.5 to 10 and from 10 to ∞.

Table 1. Natural frequencies of radial mode ω_0 and shape modes ω_k (k = 2, 3 and 4) for a bubble R_0 = 5 μm, $p_{eq} = 10^5$ Pa and β_0 = 2.5, 10, ∞. The remaining parameters are the same as in Fig. 2.

	ω_0 (MHz)	ω_2 (MHz)	ω_3 (MHz)	ω_4 (MHz)
$\beta_0 = 2.5$	94.7	2.85	4.97	7.33
$\beta_0 = 10$	9.87	2.65	4.83	7.24
$\beta_0 \rightarrow \infty$	1.93	2.65	4.83	7.24

We firstly consider the shape instability at radial resonance, for which the driving frequency is approximately equal to the natural frequency of radial oscillation. We choose ω_d = 10 and 2 MHz, which are close to ω_0 = 9.87, 1.93 for β_0 = 10 and $\beta_0 \rightarrow \infty$, respectively.

The time developments of radial mode and shape modes are shown in Fig. 3. For the cases at radial resonance (Fig. 3 (b,c)), the amplitudes of radial oscillations are dramatically larger than the ones off radial resonance (Fig. 3 (a,d)). For off radial resonance, the initial disturbances to the shape modes damp and shape instabilities do not take place. At resonance, the intense radial oscillations lead to the shape instability.

We observed two types of surface instability induced by radial resonance. In Fig. 3 (b), the third-order shape mode dominates since its natural frequency (ω_3 = 4.83 MHz) is near half of the natural frequency of the driving frequency (10 MHz), satisfying the condition of parametric instability $2\omega_k/\omega_d = 1$, as mentioned in the introduction as the one-two resonance. The dashed curve in Fig. 3 (b) presents the fact that the period of shape oscillation is approximated by twice the radial oscillation. This time scale further confirms that the instability is Mathieu's type (Hilgenfeldt et al. 1996). The shape instability in Fig. 3 (c) should be the Rayleigh-Taylor instability, because its occurrence is accompanied by a violent radial collapse and rebounding at $t/(2\pi/\omega_d) \approx 8.0$, when the lighter bubble gas expands rapidly into water (Hilgenfeldt et al. 1996). For this instability, the time scale of surface mode is much smaller than that of radial oscillation, shown as a peaked curve (dashed line).

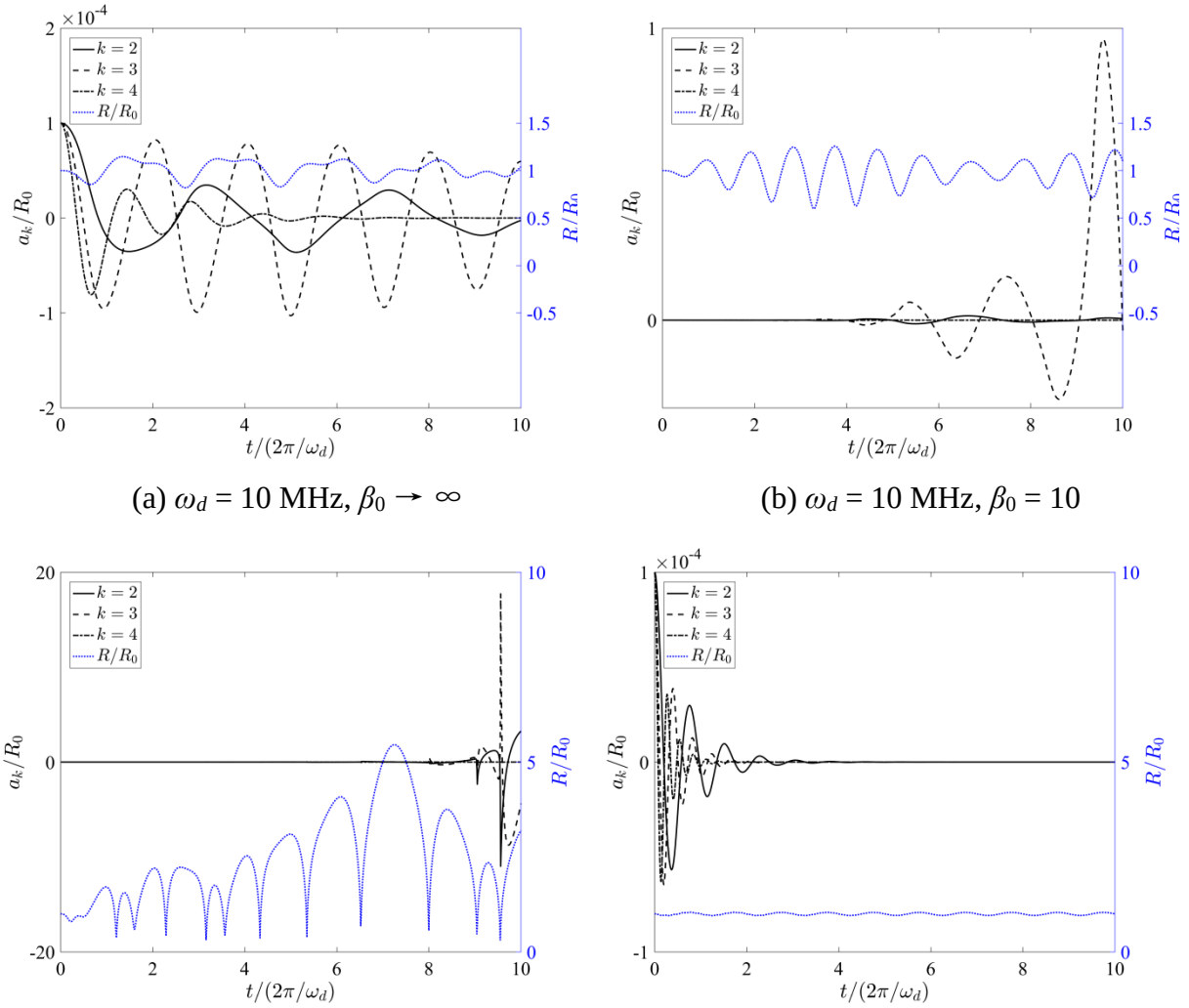

(a) ω_d = 10 MHz, $\beta_0 \to \infty$ (b) ω_d = 10 MHz, β_0 = 10

(c) ω_d = 2 MHz, $\beta_0 \to \infty$ (d) ω_d = 2 MHz, β_0 = 10

Fig. 3 Time developments of radial oscillation and shape oscillations of mode k = 2, 3 and 4 for a bubble under a driving pressure with $p_0 = 10^5$ Pa, ε = 1, ω_d = 10 MHz (a, b) and 2 MHz (c, d) for β_0 = ∞ (a, c) and 10 (b, d). The remaining parameters are the same as in Fig. 2.

Figure 4 is for a bubble in a smaller cavity, i.e. β_0 = 2.5, driven at its radial natural frequency ω_d = 95 MHz. The radial oscillation is at resonance as expected but the initial disturbance to the shape mode does not develop but eventually damps instead. This is because the confinement of a small cavity reduces the amplitude of radial oscillation due to the large effective bulk modulus for the system, making it insufficient to induce both Rayleigh-Taylor and Mathieu-type instabilities. Furthermore, the time scale of radial oscillation deviates from those of shape oscillations, which avoids the Mathieu-type instability. In a word, for a small-sized cavity, e.g. β_0 = 2.5 in the present case, shape instability does not yield even under radial resonance. By comparison, at medium-sized cavity, e.g. β_0 = 10, confinements modulate the natural frequency and thus change the driving frequency that induces shape instability.

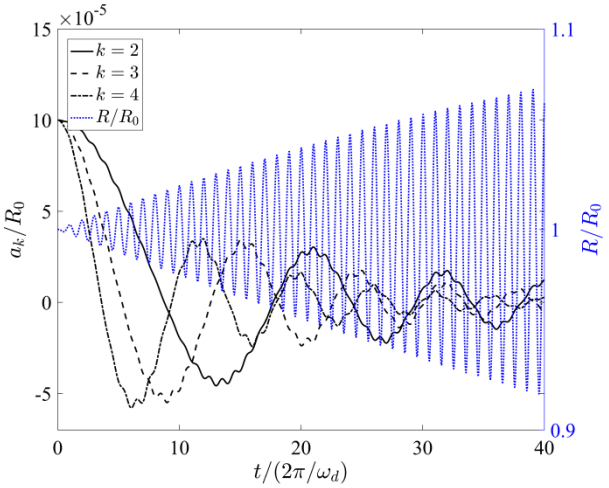

Fig. 4 Time developments of radial oscillation (blue lines) and shape oscillations of mode k = 2, 3 and 4 for a bubble under a driving pressure with $p_0 = 10^5$ Pa, $\varepsilon = 1$, ω_d = 95 MHz for $\beta_0 = 2.5$. The remaining parameters are the same as in Fig. 2.

For an unbounded bubble, the surface instability can be directly induced by resonance, with the shape mode natural frequency satisfying the parametric instability $2\omega_k/\omega_d = n$. This is most likely to happen when n = 1 or 2 (Bender & Orszag 1999), noted as one-one and one-two resonance by Feng & Leal (1993). The one-two resonance was noticed and discussed above for the appearance of k = 3 mode in Fig. 3 (b). Next we try to find out whether the one-one shape instability in confinement can be induced, by setting the driving frequencies equal to the natural frequencies of the shape mode: ω_d = 2.65 and 2.85, which are ω_2 for $\beta_0 = 2.5$ or $\beta_0 \to \infty$, respectively. The cases with ω_d = 5.3 and 5.7 MHz, which are equal to $2\omega_2$, are also presented. The Mathieu type instabilities emerge for all unconfined cases (Fig. 5 a, c, e, g) because the driving frequencies are equal or close to a multiple of its natural frequency (2.65 MHz). The time scale of shape oscillation is comparable with the radial oscillation. In contrast, the shape modes are stable for all confined cases (Figs. 5 b, d, f, h) due to the constraint of the confinement.

Figure 6 displays that the shape instability is not induced by the one-two or one-one resonance for the case with a medium confinement, e.g. $\beta_0 = 10$, whose natural frequencies of shape modes are the same as those in unbounded fluid whereas those of radial mode are five times higher. The driving frequency is thus far from the resonance frequency of radial mode and so the radius oscillates at small amplitude.

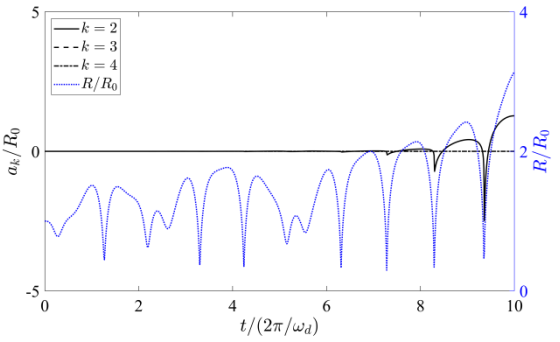

(a) ω_d = 2.65 MHz; $\beta_0 \rightarrow \infty$

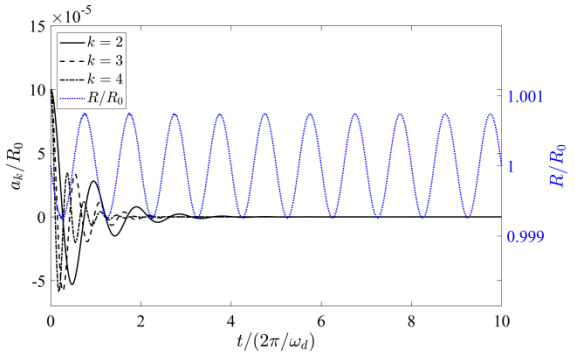

(b) ω_d = 2.65 MHz; β_0 = 2.5

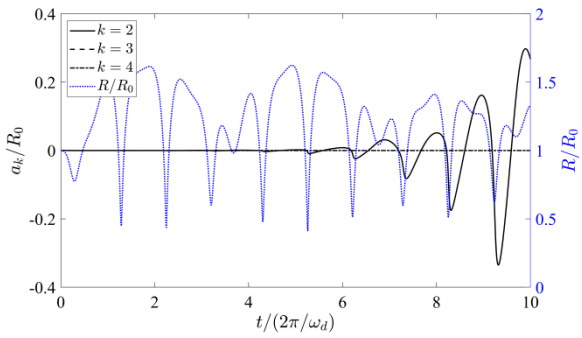

(c) ω_d = 2.85 MHz; $\beta_0 \rightarrow \infty$

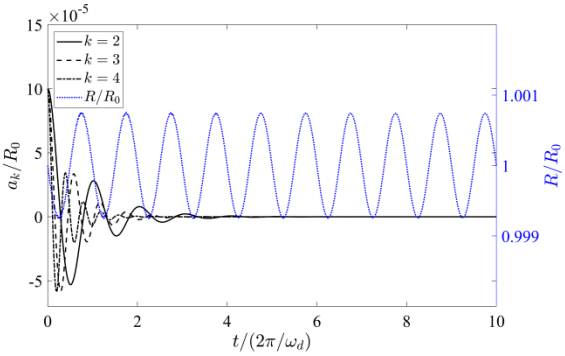

(d) ω_d = 2.85 MHz; β_0 = 2.5

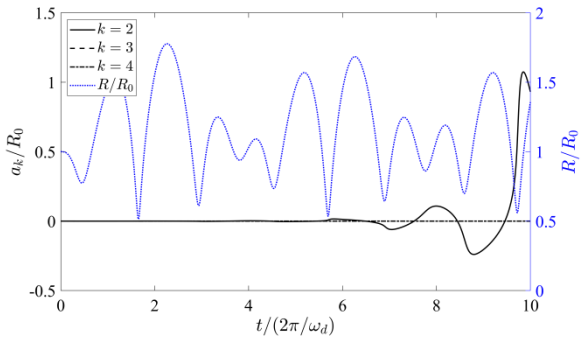

(e) ω_d = 5.3 MHz; $\beta_0 \rightarrow \infty$

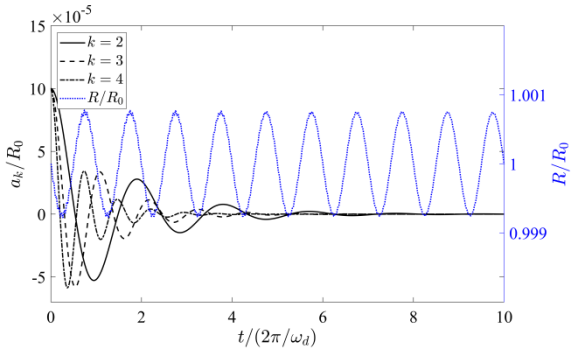

(f) ω_d = 5.3 MHz; β_0 = 2.5

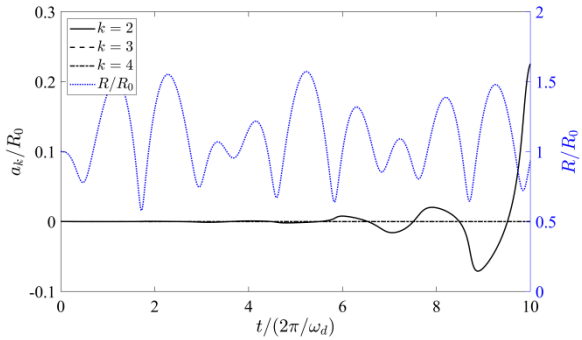

(g) ω_d = 5.7 MHz; $\beta_0 \rightarrow \infty$

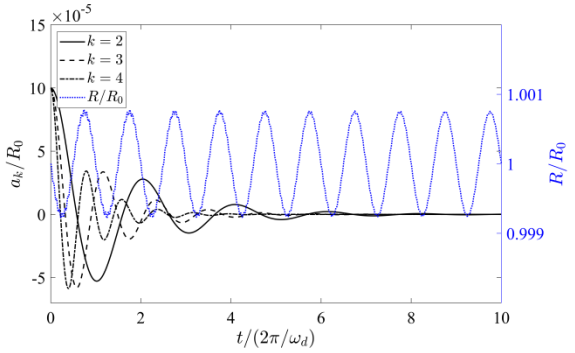

(h) ω_d = 5.7 MHz; β_0 = 2.5

Fig. 5 Time developments of radial oscillation (blue lines) and shape oscillations of mode k = 2, 3 and 4 for a bubble under a driving pressure with $p_0 = 10^5$ Pa, ε = 1, ω_d = 2.65 MHz (a, b), 2.85 MHz

(c, d), 5.3 MHz (e, f) and 5.7 MHz (g, h) for $\beta_0 = \infty$ (a, c, e, g) and 2.5 (b, d, f, h). The remaining parameters are the same as in Fig. 2.

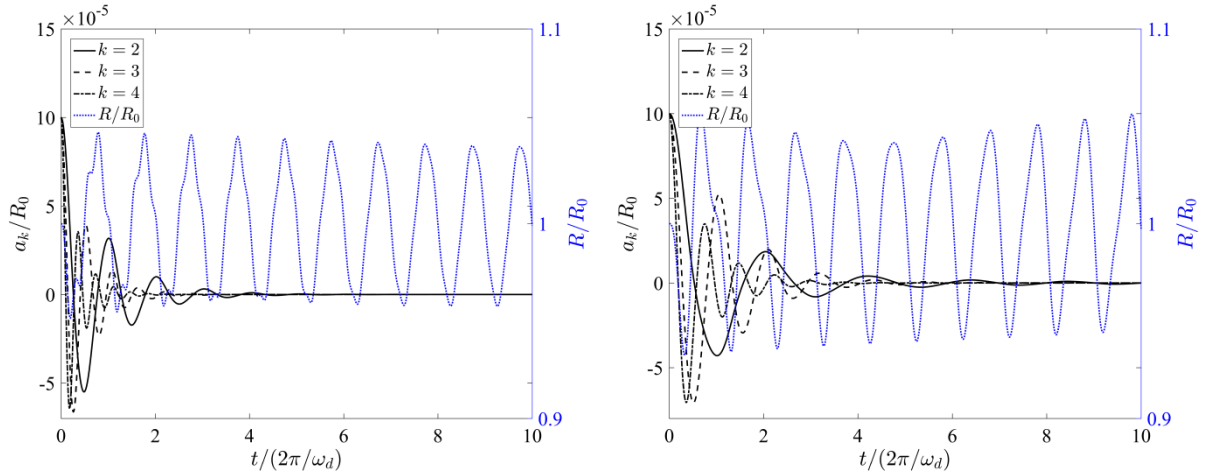

(a) ω_d = 2.65 MHz; β_0 = 10 (b) ω_d = 5.3 MHz; β_0 = 10

Fig. 6 Time developments of radial oscillation and shape oscillations of mode k = 2, 3 and 4 for a bubble under a driving pressure with $p_0 = 10^5$ Pa, ε = 1, ω_d = 2.65 MHz (a) and 5.3 MHz (b). The remaining parameters are the same as in Fig. 2.

3.3 Transient bubbles in a confinement

Next we consider the oscillation of a transient bubble which is initially at a non-equilibrium state. The initial gas pressure of a bubble with initial radius R_0 = 5 μm is set as $p_{g0} = 0.001(p_0 - p_{sat})$, where $p_0 = 10^5$ Pa is the initial pressure in liquid and p_{sat} = 2300 Pa. Due to the imbalance of the internal and external pressures, the bubble collapses initially. We investigate the effect of confinement by choosing the initial confinement ratio as β_0 = 4, 10, 20 and 40, respectively. The other parameters remain the same as shown in Fig. 2. We apply an initial disturbance to the shape modes by setting $a_k\,(t = 0)/R_0 = 10^{-4}$. The time developments of radial and shape modes are shown in Fig. 7. The results in confinements are compared with that in unbound liquid ($\beta_0 \to \infty$).

As shown in Fig. 7(a), the amplitudes of radial oscillations decrease with the confinement ratios. The bubble oscillates at much smaller amplitude for the cases of $\beta_0 \le 10$. The bubble reaches an equilibrium radius smaller than the initial radius for a large cavity, e.g. β_0 = 20 and 40 or for an unbounded field. The equilibrium radius increases and gets closer to the initial radius as the confinement effect enhances. This is because the stiffness of the system increases inversely with the cavity radius R_{c0}^3 as shown in Eq. (2.9). The initial disturbances to the shape modes for the cases of β_0 = 4 and 10 damp gradually and do not exhibit transient instabilities, as shown in Figs. 7 (b, c, d).

For β_0 = 20 and 40, the radial oscillation is at much larger amplitude and decaying with time, as shown in Fig. 7 (a) (the dashed black and red lines, respectively). Fig. 7 (b, c, d) shows that the surface instability yields almost instantly around the minimum bubble radius. This should be the Rayleigh-Taylor instability, yielded due to the rapid rebounding after the minimum bubble radius and the time scale is much smaller than the period of radial oscillation (Hilgenfeldt et al. 1996). The radius history for β_0 = 40 overlaps with the curve for an unbound liquid ($\beta_0 \to \infty$). However, their shape oscillations are not overlapped because the Rayleigh-Taylor instability exhibits chaotic characteristics.

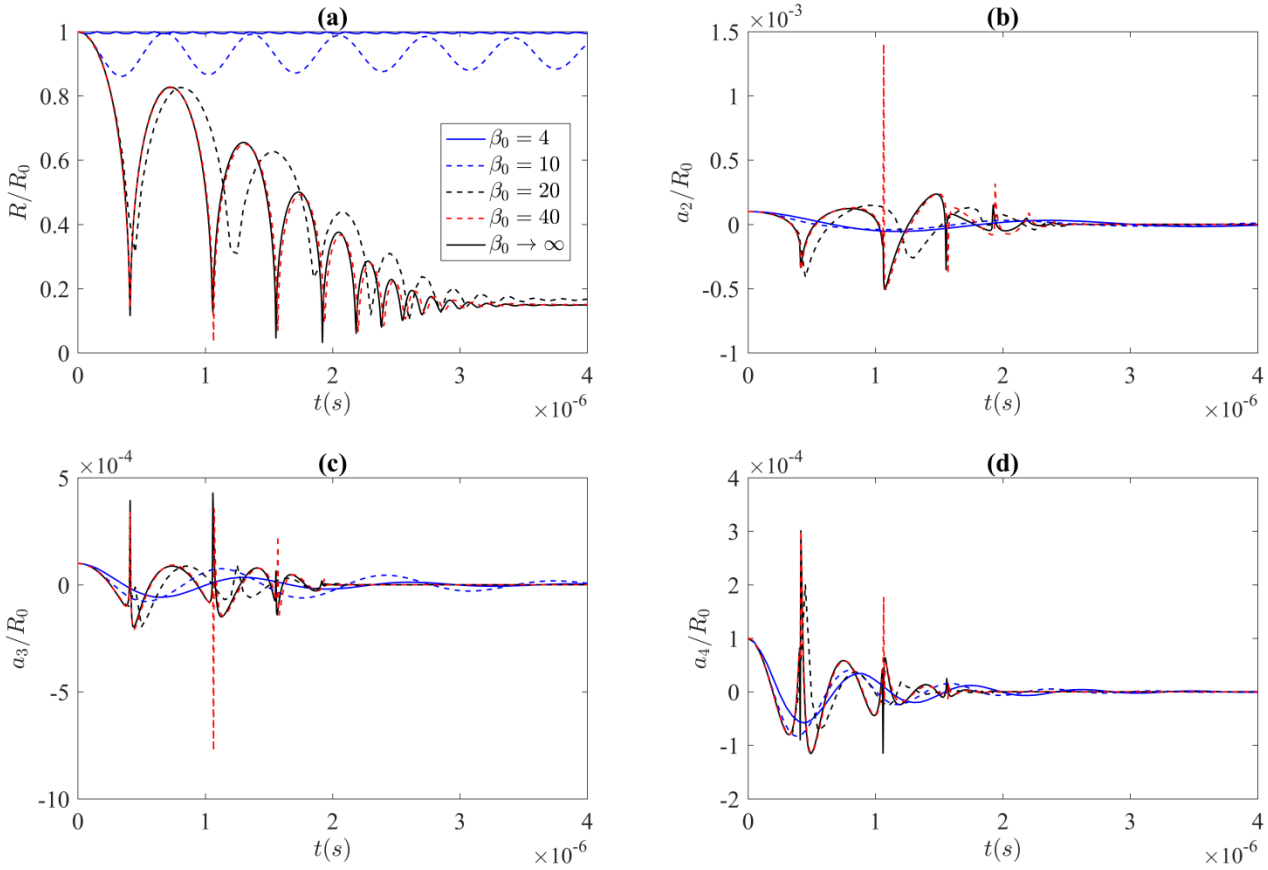

Fig. 7. Time developments of radial oscillation (a) and shape oscillations of mode k = 2 (b), 3 (c) and 4 (d) for the damped oscillation of a transient bubble. R_0 = 5 μm, p_{g0} = 0.001(p_0−p_{sat}), β_0 = ∞, 4, 10, 20 and 40. The remaining parameters are the same as in Fig. 2.

4. Summary and conclusions

In this paper we extended the classical shape mode theory to a bubble confined in a liquid-filled spherical cavity that is fully covered by elastic solid. Assumptions were made that the liquid flow was irrotational and that the relationship between the liquid pressure at the cavity surface and the

volume of the liquid or the cavity is linear. The evolution equations of shape oscillations of the confined bubble are formulated based on the Legendre polynomials. An explicit expression for the natural frequency ω_k of shape mode k is obtained as the following:

$$\omega_k / \omega_{k\infty} = \sqrt{\frac{k(\beta_{eq}^{2k+1} - 1)}{k\beta_{eq}^{2k+1} - (2k+1)\beta_{eq}^{k} + k + 1}}, \quad \omega_{k\infty} = \sqrt{\frac{\gamma(k-1)(k+1)(k+2)}{\rho R_{beq}^3}} \text{ for } k \geq 2. \qquad (4.1)$$

Analyses were conducted on the stability and the natural frequency of shape modes of bubbles with regard to the mode number, confinement size and driving frequency of acoustic waves. The features/phenomena noticed are summarized below.

The natural frequencies of a bubble increase due to the confinement and this trend is more appreciable for the radial mode than the shape modes. This is because the confinement increases the stiffness of a confined bubble system in terms of variation of volume, which is linear to radial oscillation but second order to the shape mode. The effect of confinement attenuates as the mode number increases, as this is associated with the decreasing of surface wavelength and the increase of the confinement size in terms of the wavelength.

The confinement decreases the oscillation amplitude and suppresses shape instability for both acoustic and transient bubbles. Radial resonance of a confined bubble happens when the driving frequency is equal to the natural frequency of the radial mode, which is an order of magnitude larger for a confined bubble than that for an unconfined bubble. For a small confinement $\beta_{eq} = 2.5$, the shape oscillation is stable damped. For a larger confinement $\beta_{eq} = 10$, shape mode resonance occurs when the driving frequency ω_d satisfies both the radial resonance condition, $\omega_d = \omega_0$, and the Mathieu relation $\omega_d = 2\omega_k/n$, where n is a natural number. These findings are of great relevance in medical application for which the surface stability is important and is usually controlled by detuning acoustic frequency

A transient confined bubble undergoes stable damped oscillation for $\beta_0 \leq 10$. For $\beta_0 \geq 20$, the bubble oscillates at a much larger amplitude, which may lead to the Rayleigh–Taylor instability for the shape mode during violent rebounding.

For simplification in analysis, assumptions are made that the cavity and the bubble are spherical and concentric. Some of the results obtained here are expected to stand qualitatively for general cases, including: The natural frequency of shape mode increasing appreciably only if the cavity dimension is within 2-3 bubble radii, when the shape oscillation is always stable and damps with time; The natural frequency of shape mode should not change significantly due to the presence of boundaries when the standoff distance of the bubble to the boundaries is more than 2-3 bubble radii. As the cavity dimension is 10 times larger than the bubble radius, the natural frequency for radial oscillation is significantly larger and the natural frequency for shape mode remains the same

as that for an unconfined bubble; shape instability of a confined bubble can only be activated when both the radial resonance and shape resonance conditions are satisfied.

Acknowledgements

This work was supported by the National Natural Science Foundation of China through Grant No.11772196 and by the Engineering and Physical Sciences Research Council (EPSRC) through Grant No. EP/P015743/1.

Appendix A Derivation of the kinematic boundary condition Eq. (2.15)

The velocity potential Eq. (2.10) and the kinematic boundary condition Eq. (2.11) are rewritten here,

$$\varphi(r,\theta,t)=\frac{A_0(t)}{r}+B_0(t)+\sum_{k=2}^{\infty}\left[\frac{A_k(t)}{r^{k+1}}+B_k(t)r^k\right]P_k(\cos\theta), \tag{2.10}$$

$$\frac{\partial S}{\partial t}+(\nabla\varphi\cdot\nabla)S=0. \tag{2.11}$$

Notice the the bubble interface S_b has been defined as $S_b=r-R_b(t)-\sum_{k=2}^{\infty}a_k(t)P_k(\cos\theta)$. The time derivative to the surface function is

$$\frac{\partial S_b}{\partial t}=-\dot{R}_b-\sum_{k=2}^{\infty}\dot{a}_kP_k(\cos\theta). \tag{A1}$$

The gradient to the surface function is

$$\nabla S_b=\frac{\partial S_b}{\partial r}\mathbf{e}_r+\frac{1}{r}\frac{\partial S_b}{\partial\theta}\mathbf{e}_\theta=\mathbf{e}_r-\mathbf{e}_\theta\sum_{k=2}^{\infty}\frac{a_k}{r}P_k^1(\cos\theta), \tag{A2}$$

where $P_k^1(\cos\theta)=dP_k(\cos\theta)/d\theta$ is the associated Legendre polynomials.

Similarly, we write the gradient to the velocity explicitly as

$$\nabla\varphi=\frac{\partial\varphi}{\partial r}\mathbf{e}_r+\frac{1}{r}\frac{\partial\varphi}{\partial\theta}\mathbf{e}_\theta, \tag{A3}$$

where

$$\frac{\partial\varphi}{\partial r}=-\frac{A_0}{r^2}+\sum_{k=2}^{\infty}\left[-(k+1)\frac{A_k}{r^{k+2}}+kB_kr^{k-1}\right]P_k(\cos\theta), \tag{A4}$$

$$\frac{1}{r}\frac{\partial\varphi}{\partial\theta}=\sum_{k=2}^{\infty}\left[\frac{A_k}{r^{k+2}}+B_kr^{k-1}\right]P_k^1(\cos\theta). \tag{A5}$$

The second term of Eq. (2.11) is written as

$$(\nabla\varphi\cdot\nabla)S=\frac{\partial\varphi}{\partial r}\frac{\partial S}{\partial r}+\frac{1}{r}\frac{\partial\varphi}{\partial\theta}\frac{1}{r}\frac{\partial S}{\partial\theta}. \tag{A6}$$

Substituting Eqs. (A2), (A4) and (A5) into (A6), expanding in terms of $r=R_b(t)+\sum_{k=2}^{\infty}a_k(t)P_k(\cos\theta)$ and keeping the terms up to the order of $O(a_k)$, i.e. only considering the linear stability of the shape mode, we have

$$\begin{aligned}(\nabla\varphi\cdot\nabla)S&=-\frac{A_0}{r^2}+\sum_{k=2}^{\infty}\left[-(k+1)\frac{A_k}{r^{k+2}}+kB_k r^{k-1}\right]P_k(\cos\theta)\\&=-\frac{A_0}{R_b{}^2}+\sum_{k=2}^{\infty}\left[\frac{2A_0}{R_b{}^3}a_k-(k+1)\frac{A_k}{R_b{}^{k+2}}+kB_k R_b{}^{k-1}\right]P_k(\cos\theta).\end{aligned} \tag{A7}$$

Substituting Eqs. (A1) and (A7) into (2.11), we obtain the kinematic boundary at the bubble interface explicitly Eq. (2.15).

Appendix B Derivation of the dynamic conditions Eqs. (2.26) and (2.28)

The Bernoulli equation (2.22) for the liquid flow is rewritten as

$$\rho\left(\frac{\partial\varphi}{\partial t}+\frac{1}{2}|\nabla\varphi|^2\right)_{S_b}+p_{lb}=\rho\left(\frac{\partial\varphi}{\partial t}+\frac{1}{2}|\nabla\varphi|^2\right)_{S_c}+p_c. \tag{2.22}$$

In this appendix, we provide the detailed derivation to the terms related to the velocity potential. The terms relevant to the bubble interface will be expanded in terms of $r=R_b(t)+\sum_{k=2}^{\infty}a_k(t)P_k(\cos\theta)$, keeping the terms up to $O(a_k)$. The velocity potential has been defined in Eq. (2.10). The time derivative to the velocity potential is

$$\frac{\partial\varphi}{\partial t}=\frac{\dot{A}_0}{r}+\sum_{k=2}^{\infty}\left[\frac{\dot{A}_k}{r^{k+1}}+\dot{B}_k r^k\right]P_k(\cos\theta). \tag{B1}$$

At the bubble interface,

$$\left.\frac{\partial\varphi}{\partial t}\right|_{S_b}=\frac{\dot{A}_0}{R_b}+\sum_{k=2}^{\infty}\left[-\frac{\dot{A}_0}{R_b{}^2}+\frac{\dot{A}_k}{R_b{}^{k+1}}+\dot{B}_k R_b{}^k\right]P_k(\cos\theta). \tag{B2}$$

At the cavity,

$$\left.\frac{\partial\varphi}{\partial t}\right|_{S_c}=\frac{\dot{A}_0}{R_c}+\sum_{k=2}^{\infty}\left[\frac{\dot{A}_k}{R_c{}^{k+1}}+\dot{B}_k R_c{}^k\right]P_k(\cos\theta). \tag{B3}$$

The second term in Eq. (2.22) is expressed as

$$\frac{1}{2}|\nabla\varphi|^2=\frac{1}{2}\left[\left(\frac{\partial\varphi}{\partial r}\right)^2+\left(\frac{1}{r}\frac{\partial\varphi}{\partial\theta}\right)^2\right]. \tag{B4}$$

According to the expression (A5) and the rule of keeping the terms up to $O(a_k)$, the second term in the right hand side of (B4) is eliminated. The first term is written using Eq. (A4) as

$$\frac{1}{2}\left(\frac{\partial\varphi}{\partial r}\right)^2=\frac{1}{2}\frac{A_0^{\,2}}{r^4}+\sum_{k=2}^{\infty}\left[(k+1)\frac{A_0A_k}{r^{k+4}}-kA_0B_kr^{k-3}\right]P_k(\cos\theta). \tag{B5}$$

At the bubble interface,

$$\frac{1}{2}\left(\frac{\partial\varphi}{\partial r}\right)^2\bigg|_{S_b}=\frac{1}{2}\frac{A_0^{\,2}}{R_b^{\,4}}+\sum_{k=2}^{\infty}\left[-\frac{2A_0^{\,2}}{R_b^{\,5}}a_k+(k+1)\frac{A_0A_k}{R_b^{\,k+4}}-kA_0B_kR_b^{\,k-3}\right]P_k(\cos\theta). \tag{B6}$$

At the cavity,

$$\frac{1}{2}\left(\frac{\partial\varphi}{\partial r}\right)^2\bigg|_{S_c}=\frac{1}{2}\frac{A_0^{\,2}}{R_c^{\,4}}+\sum_{k=2}^{\infty}\left[(k+1)\frac{A_0A_k}{R_c^{\,k+4}}-kA_0B_kR_c^{\,k-3}\right]P_k(\cos\theta) \tag{B7}$$

Equation (2.23) indicates that the dynamic boundary condition on the bubble surface decides p_{lb}, the pressure of the liquid on the bubble-liquid surface in equation (2.22), and equation (2.23) can be transformed into

$$-p_{lb}-p_A+2\mu\frac{\partial^2\varphi}{\partial r^2}=-p_B+\gamma\nabla\cdot\mathbf{n}, \tag{2.23}$$

where

$$\begin{aligned}\frac{\partial^2\varphi}{\partial r^2}&=2\frac{A_0}{r^3}+\sum_{k=2}^{\infty}\left[-(k+1)(k+2)\frac{A_k}{r^{k+3}}+k(k-1)B_kr^{k-2}\right]P_k(\cos\theta)\\&=2\frac{A_0}{R_b^{\,3}}+\sum_{k=2}^{\infty}\left[-\frac{6A_0}{R_b^{\,4}}a_k-(k+1)(k+2)\frac{A_k}{R_b^{\,k+3}}+k(k-1)B_kR_b^{\,k-2}\right]P_k(\cos\theta).\end{aligned} \tag{B8}$$

Collecting Eqs. (B2), (B3), (B4) and (2.23), (2.24), (2.25) into (2.22), and making use of the orthogonality of the Legendre polynomial, we obtain the dynamic equations (2.26) and (2.28).

REFERENCES

Asaki, T. J., Marston, P. L. and Trinh, E. H. 1993 Shape oscillations of bubbles in water driven by modulated ultrasonic radiation pressure: observations and detection with scattered laser light. J. Acoust. Soc. Am. 93 706–713

Asaki, T. J. and Marston, P. L. 1995 Free decay of shape oscillations of bubbles acoustically trapped in water and sea water J. Fluid Mech. 300 149–67

Bender, C. M. and Orszag, 1999 Advanced mathematical methods for scientists and engineers: Asymptotic methods and perturbation theory, Sringer-Verlag, New York.

Benjamin, T. B. 1964 Surface effects in non-spherical motions of small cavities. In Cavitation in

Real Liquids, Elsevier 164-180.

Bjerknes, K., Sontum, P. C., Smistad, G., and Agerkvista, I. 1997 Preparation of polymeric microbubbles: Formulation studies and product characterization, Int. J. Pharm 158, 129-136.

Brennen, C. E. 1995 Cavitation and Bubble Dynamics, Oxford University Press (available online).

Brenner, M. P., Hilgenfeldt, S. and Lohse, D. 2002 Single-bubble sonoluminescence, Rev. Mod. Phys. 74, 425–484.

Dollet, B., van der Meer, S. M., Garbin, V., de Jong, N., Lohse, D. and Versluis, M. 2008 Nonspherical oscillations of ultrasound contrast agent microbubbles, Ultrasound Med. Biol. 34, 1465–1473.

Feng, Z. X. and Leal, L. G. 1993 On energy transfer in resonanct bubble oscillations. Phys. Fluids A 5, 826-836.

Feng, Z. C. and Leal, L.G. 1997 Nonlinear bubble dynamics. Annu. Rev. Fluid Mech. 29 201–43.

Fourest, T., Laurens, J., Deletombe, E., Dupas, J. and Arrigoni, M. 2014 Analysis of bubbles dynamics created by hydrodynamic ram in confined geometries using the Rayleigh-Plesset equation. Int. J. Impact Eng. 73, 66-74.

Hilgenfeldt, S., Lohse, D. and Brenner, M. P. 1996 Phase diagrams for sonoluminescing bubbles, Phys. Fluids 8(11), 2808–2826.

Knapp, R. T., Daili, J. W. and Hammit, F. G. 1970 Cavitation. New York: Mc Graw Hill Book Company.

Lamb, H. 1932 Hydrodynaimics. Cambridge University Press.

Lauterborn, W. and Kurz, T. 2010 Physics of bubble oscillations. Rep. Prog. Phys. 73, 10650.

Marmottant, P. and Hilgenfeldt, S. 2004 A bubble-driven microfluidic transport element for bioengineering. *Proc. Natl. Acad. Sci.* 101. 9523-9527.

Marti, D., Kruger, Y., Fleitmann, D., Frenz, M. and Ricka, J. 2012 The effect of surface tension on liquid-gas equilibria in isochoric systems and its application to fluid inclusions. Fluid Physe Equilib. 314, 13-21.

Martynov, S., Stride, E. & Saffari, N. 2009 The natural frequencies of microbubble oscillation in elastic vessels. J. Acoust. Soc. Am. 126 (6), 2963–2972.

Minnaert, M. 1933 On musical sir-bubbles and the sound of running water. Phil. Mag. 16, 235-248.

Noblin, X. Rojas, N. O., Westbrook, J., Llorens, C., Argentina, M. and Dumais, J. 2012 The fern sporangium: A unique catapult. Science 335, 1322.

Roedder, E. and Bodnar, R. J. Geologic pressure determinations rom fluid inclusion studies. 1980 Anuu. Rev. Earth Planet. Sci.8, 263-301.

De Roo, L., Vergeynst, L. L., De Baerdemaeker, N. J. F. and Steppe, K. 2016 Acoustic emissions to measure drought-induced cavitation in plants. Appl. Sci. 6(3), 71.

Plesset, M. S. 1954 On the stability of fluid flows with spherical symmetry. J. Appl. Phys. 25, 96-98.

Plesset, M. S. and Prosperetti, A. 1977 Bubble dynamics and cavitation. Ann. Rev. Fluid Mech. 9, 145-185.

Sharp, D. H. 1984 An overview of Rayleigh-Taylor instability. Physica D: Nonlinear Phenomena 12, 3-18.

Soltani, H., Sabbagh, R. and Nobes, D. S. 2018 The passage of bubbles rising through a confining rectangular geometry, Phys. Fluids 30, 103302.

Tyree, M. T. and Sperry, J. S. 1989 Vulnerability of xylem to cavitation and embolism. Annu. Rev. Plant Phys. Mol. Bio. 1989, 40, 19-38.

Versluis, M., Goertz, D. E., Palanchon, P., Heitman, I. L., van der Meer, S. M., Dollet, B., de Jong, N., and Lohse, D. 2010 Microbubble shape oscillations excited through ultrasonic parametric driving. Phys. Rev. E 82, 026321.

Vincent, O. and Marmottant, P. 2017 On the statics and dynamics of fully confined bubbles. J. Fluid Mech. 827, 194-224.

Vincent, O., Marmottant, P., Gonzalez-Avila, S. R., Ando, K. and Ohl, C. D. 2014 The fast dynamics of cavitation bubbles within water confined in elastic solids. Soft Matter 10, 1455–1461.

Wang, Q. X. 2017 Oscillation of a bubble in a liquid confined in an elastic solid. Phys. Fluid 29, 072101.

Yang, S. M., Feng, Z. C. and Leal, L. G. 1993 Nonlinear effects in the dynamics of shape and volume oscillations for a gas bubble in an external flow. J. Fluid Mech. 247, 417-454.